

Histogram of Gradient Orientations of Signal Plots applied to P300 Detection

Rodrigo Ramele^{1,*}, Ana Julia Villar¹ and Juan Miguel Santos¹

¹*Centro de Inteligencia Computacional, Computer Engineering Department,
Instituto Tecnológico de Buenos Aires, Buenos Aires, Argentina*

Correspondence*:

Rodrigo Ramele, C1437FBH Lavarden 315, Ciudad Autónoma de Buenos Aires,
Argentina
rramele@itba.edu.ar

2 ABSTRACT

3 Word Count: 4952

4 The analysis of Electroencephalographic (EEG) signals is of ulterior importance to aid in the
5 diagnosis of mental disease and to increase our understanding of the brain. Traditionally, clinical
6 EEG has been analyzed in terms of temporal waveforms, looking at rhythms in spontaneous
7 activity, subjectively identifying troughs and peaks in Event-Related Potentials (ERP), or by
8 studying graphoelements in pathological sleep stages. Additionally, the discipline of Brain
9 Computer Interfaces requires new methods to decode patterns from non-invasive EEG signals.
10 This field is developing alternative communication pathways to transmit volitional information
11 from the Central Nervous System. The technology could potentially enhance the quality of life
12 of patients affected by neurodegenerative disorders and other mental illness. This work mimics
13 what electroencephalographers have been doing clinically, visually inspecting and categorizing
14 phenomena within the EEG by the extraction of features from images of signal plots, but aims to
15 provide a new objective framework to analyze, characterize and classify EEG signal waveforms.
16 These features are constructed based on the calculation of histograms of the oriented gradients
17 from pixels around the signal plot. The feasibility of the method is outlined by detecting the
18 P300, an ERP elicited by the oddball paradigm of rare events, and implementing an offline
19 P300-based BCI Speller. The validity of the proposal is shown by offline processing a public
20 dataset of Amyotrophic Lateral Sclerosis (ALS) patients and an own dataset of healthy subjects.

21 **Keywords:** electroencephalography, histogram of gradient orientations, brain-computer interfaces, P300, SIFT, amyotrophic lateral
22 sclerosis, naive-bayes near neighbours, waveforms

1 INTRODUCTION

23 Although recent advances in neuroimaging techniques, particularly radio-nuclear and radiological
24 scanning methods (Schomer and Silva, 2010), have diminished the prospects of the traditional
25 Electroencephalography (EEG), the advent and development of digitized devices has impelled for a
26 revamping of this hundred years old technology. Their versatility, ease of use, temporal resolution, ease of
27 development and production, and its proliferation as consumer devices, are pushing EEG to become the
28 de-facto non invasive portable or ambulatory method to access and harness brain information (De Vos and
29 Debener, 2014).

30 A key contribution to this expansion has been the field of Brain Computer Interfaces (BCI) (Wolpaw and
31 E., 2012) which is the pursuit of the development of a new channel of communication particularly aimed to
32 persons affected by neurodegenerative diseases.

33 One noteworthy aspect of this novel communication channel is the ability to transmit information from
34 the Central Nervous System (CNS) to a computer device and from there use that information to control a
35 wheelchair (Carlson and del R. Millan, 2013), as input to a speller application (Guger et al., 2009), in a
36 Virtual Reality environment (Lotte et al., 2013) or as aiding tool in a rehabilitation procedure (Jure et al.,
37 2016). The holly grail of BCI is to implement a new complete and alternative pathway to restore lost
38 locomotion (Wolpaw and E., 2012).

39 EEG signals are remarkably complex and have been characterized as a multichannel non-stationary
40 stochastic process. Additionally, they have high variability between different subjects and even between
41 different moments for the same subject, requiring adaptive and co-adaptive calibration and learning
42 procedures (Clerc et al., 2016). Hence, this imposes an outstanding challenge that is necessary to overcome
43 in order to extract information from raw EEG signals.

44 BCI has gained mainstream public awareness with worldwide challenge competitions like
45 Cybathlon (Riener and Seward, 2014; Novak et al., 2018) and even been broadcasted during the inauguration
46 ceremony of the 2014 Soccer World Cup. New developments have overcome the out-of-the-lab high-bar
47 and they are starting to be used in real world environments (Guger et al., 2017; Huggins et al., 2016).
48 However, they still lack the necessary robustness, and its performance is well behind any other method of
49 human computer interaction, including any kind of detection of residual muscular movement (Clerc et al.,
50 2016).

51 A few works have explored the idea of exploiting the signal waveform to analyze the EEG signal.
52 In (Alvarado-González et al., 2016) an approach based on Slope Horizontal Chain Code is presented,
53 whereas in (Yamaguchi et al., 2009) a similar procedure was implemented based on Mathematical
54 Morphological Analysis. The seminal work of Bandt-Pompe Permutation Entropy (Berger et al., 2017) also
55 explores succinctly this idea as a basis to establish the time series ordinal patterns. In the article (Ramele
56 et al., 2016), the authors introduce a method for classification of rhythmic EEG events like Visual Occipital
57 Alpha Waves and Motor Imagery Rolandic Central μ Rhythms using the Histogram of Gradient Orientations
58 of signal plots. Inspired in that work, we propose a novel application of the developed method to classify
59 and describe transient events, particularly the P300 Event Related Potential. The proposed approach is
60 based on the waveform analysis of the shape of the EEG signal. The signal is drawn on a bidimensional
61 image plot, vector gradients of pixels around the plot are obtained, and with them, the histogram of their
62 orientations is calculated. This histogram is a direct representation of the waveform of the signal. The
63 method is built by mimicking what regularly electroencephalographers have been performing for almost a
64 century as it is described in (Hartman, 2005): visually inspecting raw signal plots.

65 This paper reports a method to, (1) describe a procedure to capture the shape of a waveform of an ERP
66 component, the P300, using histograms of gradient orientations extracted from images of signal plots,
67 and (2) outline the way in which this procedure can be used to implement an P300-Based BCI Speller
68 application. Its validity is verified by offline processing two datasets, one of data from ALS patients and
69 another one from data of healthy subjects.

70 This article unfolds as follows: Section 2.1 is dedicated to explain the Feature Extraction method based
71 on Histogram of Gradient Orientations of the Signal Plot: Section 2.1.1 shows the preprocessing pipeline,
72 Section 2.1.2 describes the image generation of the signal plot, Section 2.1.3 presents the feature extraction

73 procedure while Section 2.1.4 introduces the Speller Matrix Letter Identification procedure. In Section 2.2,
74 the experimental protocol is expounded. Section 3 shows the results of applying the proposed technique. In
75 the final Section 4 we expose our remarks, conclusions and future work.

2 MATERIALS AND METHODS

76 The P300 (Farwell and Donchin, 1988; Knuth et al., 2006) is a positive deflection of the EEG signal which
77 occurs around 300 ms after the onset of a rare and deviant stimulus that the subject is expected to attend. It
78 is produced under the oddball paradigm (Wolpaw and E., 2012) and it is consistent across different subjects.
79 It has a lower amplitude ($\pm 5\mu V$) compared to basal EEG activity, reaching a Signal to Noise Ratio (SNR)
80 of around -15 db estimated based on the amplitude of the P300 response signal divided by the standard
81 deviation of the background EEG activity (Hu et al., 2010). This signal can be used to implement a speller
82 application by means of a Speller Matrix (Farwell and Donchin, 1988). This matrix is composed of 6 rows
83 and 6 columns of numbers and letters. The subject can focus on one character of the matrix. Figure 1 shows
84 an example of the Speller Matrix used in the OpenVibe open source software (Renard et al., 2010), where
85 the flashes of rows and columns provide the deviant stimulus required to elicit this physiological response.
86 Each time a row or a column that contains the desired letter flashes, the corresponding synchronized EEG
87 signal should also contain the P300 signature and by detecting it, the selected letter can be identified.

88 2.1 Feature Extraction from Signal Plots

89 In this section, the signal preprocessing, the method for generating images from signal plots, the feature
90 extraction procedure and the Speller Matrix identification are described. Figure 2 shows a scheme of the
91 entire process.

92 2.1.1 Preprocessing Pipeline

93 The data obtained by the capturing device is digitalized and a multichannel EEG signal is constructed.
94 The 6 rows and 6 columns of the Speller Matrix are intensified providing the visual stimulus. The
95 number of a row or column is a location. A sequence of twelve randomly permuted locations l conform an
96 intensification sequence. The whole set of twelve intensifications is repeated k_a times.

97 • **Signal Enhancement:** This stage consists of the enhancement of the SNR of the P300 pattern above
98 the level of basal EEG. The pipeline starts by applying a notch filter to the raw digital signal, a 4th
99 degree 10 Hz lowpass Butterworth filter and finally a decimation with a Finite Impulse Response (FIR)
100 filter of order 30 from the original sampling frequency down to 16 Hz (Krusienski et al., 2006).

101 • **Artifact Removal:** For every complete sequence of 12 intensifications of 6 rows and 6 columns, a
102 basic artifact elimination procedure is implemented by removing the entire sequence when any signal
103 deviates above/below $\pm 70\mu V$.

104 • **Segmentation:** For each of the 12 intensifications of one intensification sequence, a segment S_i^l
105 of a window of t_{max} seconds of the multichannel signal is extracted, starting from the stimulus
106 onset, corresponding to each row/column intensification l and to the intensification sequence i . As
107 intensifications are permuted in a random order, the segments are rearranged corresponding to row
108 flickering, labeled 1-6, whereas those corresponding to column flickering are labeled 7-12. Two of
109 these segments should contain the P300 ERP signature time-locked to the flashing stimulus, one for
110 the row, and one for the column.

111 • **Signal Averaging:** The P300 ERP is deeply buried under basal EEG so the standard approach to
 112 identify it is by point-to-point averaging the time-locked stacked signal segments. Hence the values
 113 which are not related to, and not time-locked to the onset of the stimulus are canceled out (Liang and
 114 Bougrain, 2008).

115 This last step determines the operation of any P300 Speller. In order to obtain an improved signal
 116 in terms of its SNR, repetitions of the sequence of row/column intensification are necessary. And,
 117 at the same time, as long as more repetitions are needed, the ability to transfer information faster is
 118 diminished, so there is a trade-off that must be acutely determined.

119 The procedure to obtain the point-to-point averaged signal goes as follows:

- 120 1. Highlight randomly the rows and columns from the matrix. There is one row and one column that
 121 should match the letter selected by the subject.
- 122 2. Repeat step 1 k_a times, obtaining the $1 \leq l \leq 12$ segments $S_1^l(n, c), \dots, S_{k_a}^l(n, c)$, of the EEG
 123 signal where the variables $1 \leq n \leq n_{max}$ and $1 \leq c \leq C$ correspond to sample points and channel,
 124 respectively. The parameter C is the number of available EEG channels whereas $n_{max} = F_s t_{max}$
 125 is the segment length and F_s is the sampling frequency. The parameter k_a is the number of
 126 repetitions of intensifications and it is an input parameter of the algorithm.
- 127 3. Compute the Ensemble Average by

$$x^l(n, c) = \frac{1}{k_a} \sum_{i=1}^{k_a} S_i^l(n, c) \quad (1)$$

128 for $1 \leq n \leq n_{max}$ and for the channels $1 \leq c \leq C$. This provide an averaged signal $x^l(n, c)$ for
 129 the twelve locations $1 \leq l \leq 12$.

130 2.1.2 Signal Plotting

131 Averaged signal segments are standardized and scaled for $1 \leq n \leq n_{max}$ and $1 \leq c \leq C$ by

$$\tilde{x}^l(n, c) = \left[\gamma \frac{(x^l(n, c) - \bar{x}^l(c))}{\hat{\sigma}^l(c)} \right] \quad (2)$$

where $\gamma > 0$ is an input parameter of the algorithm and it is related to the image scale. In addition, $x^l(n, c)$ is the point-to-point averaged multichannel EEG signal for the sample point n and for channel c . Lastly,

$$\bar{x}^l(c) = \frac{1}{n_{max}} \sum_{n=1}^{n_{max}} x^l(n, c)$$

and

$$\hat{\sigma}^l(c) = \left(\frac{1}{n_{max} - 1} \sum_{n=1}^{n_{max}} (x^l(n, c) - \bar{x}^l(c))^2 \right)^{\frac{1}{2}}$$

132 are the mean and estimated standard deviation of $x^l(n, c)$, $1 \leq n \leq n_{max}$, for each channel c .

133 Consequently, a binary image $I^{(l,c)}$ is constructed according to

$$I^{(l,c)}(z_1, z_2) = \begin{cases} 255 & \text{if } z_1 = \gamma n; z_2 = \tilde{x}^l(n, c) + z^l(c) \\ 0 & \text{otherwise} \end{cases} \quad (3)$$

134 with 255 being white and representing the signal's value location and 0 for black which is the background
 135 contrast, conforming a black-and-white plot of the signal. Pixel arguments $(z_1, z_2) \in \mathbb{N} \times \mathbb{N}$ iterate over
 136 the width (based on the length of the signal segment) and height (based on the peak-to-peak amplitude) of
 137 the newly created image with $1 \leq n \leq n_{max}$ and $1 \leq c \leq C$. The value $z^l(c)$ is the image vertical position
 138 where the signal's zero value has to be situated in order to fit the entire signal within the image for each
 139 channel c :

$$z^l(c) = \left\lfloor \frac{\max_n \tilde{x}^l(n, c) - \min_n \tilde{x}^l(n, c)}{2} \right\rfloor - \left\lfloor \frac{\max_n \tilde{x}^l(n, c) + \min_n \tilde{x}^l(n, c)}{2} \right\rfloor \quad (4)$$

140 where the minimization and maximization are carried out for n varying between $1 \leq n \leq n_{max}$, and $\lfloor \cdot \rfloor$
 141 denote the rounding to the smaller nearest integer of the number.

142 In order to complete the plot $I^{(l,c)}$ from the pixels, the Bresenham (Bresenham, 1965; Ramele et al.,
 143 2016) algorithm is used to interpolate straight lines between each pair of consecutive pixels.

144 2.1.3 Feature Extraction: Histogram of Gradient Orientations

145 For each generated image $I^{(l,c)}$, a keypoint \mathbf{p}_k is placed on a pixel (x_{p_k}, y_{p_k}) over the image plot and a
 146 window around the keypoint is considered. A local image patch of size $X_p \times X_p$ pixels is constructed by
 147 dividing the window in 16 blocks of size $3s$ each one, where s is the scale of the local patch and it is an
 148 input parameter of the algorithm. It is arranged in a 4×4 grid and the pixel \mathbf{p}_k is the patch center, thus
 149 $X_p = 12s$ pixels.

150 A local representation of the signal shape within the patch can be described by obtaining the gradient
 151 orientations on each of the 16 blocks $B_{i,j}$ with $0 \leq i, j \leq 3$ and creating a histogram of gradients. This
 152 technique is based on Lowe's SIFT (Lowe, 2004) method, and it is biomimetically inspired in how the
 153 visual cortex detects shapes by analyzing orientations (Edelman et al., 1997). In order to calculate the
 154 histogram, the interval $[0, 360]$ of possible angles is divided in 8 bins, each one of 45 degrees.

155 Hence, for each spatial bin $0 \leq i, j \leq 3$, corresponding to the indexes of each block $B_{i,j}$, the orientations
 156 are accumulated in a 3-dimensional histogram h through the following equation:

$$h(\theta, i, j) = 3s \sum_{\mathbf{p} \in I^{(l,c)}} w_{ang}(\angle J(\mathbf{p}) - \theta) w_{ij} \left(\frac{\mathbf{p} - \mathbf{p}_k}{3s} \right) |J(\mathbf{p})| \quad (5)$$

157 where \mathbf{p} is a pixel from the image $I^{(l,c)}$, θ is the angle bin with $\theta \in \{0, 45, 90, 135, 180, 225, 270, 315\}$,
 158 $|J(\mathbf{p})|$ is the norm of the gradient vector in the pixel \mathbf{p} and it is computed using finite differences and $\angle J(\mathbf{p})$
 159 is the angle of the gradient vector. The scalar $w_{ang}(\cdot)$ and vector $w_{ij}(\cdot)$ functions are linear interpolations
 160 used by Lowe (2004) and Vedaldi and Fulkerson (2010) to provide a weighting contribution to eight
 161 adjacent bins. They are calculated as

$$w_{ij}(\mathbf{v}) = w(v_x - x_i)w(v_y - y_j) \quad (6)$$

162 with $0 \leq i, j \leq 3$ and

$$w_{\text{ang}}(\alpha) = \sum_{r=-1}^1 w\left(\frac{8\alpha}{2\pi} + 8r\right) \quad (7)$$

163 where x_i and y_i are the spatial bin centers located in $x_i, y_j \in \{-\frac{3}{2}, -\frac{1}{2}, \frac{1}{2}, \frac{3}{2}\}$, $\mathbf{v} = (v_x, v_y)$ is a vector
 164 variable and α a scalar variable. On the other hand, r is an integer that can vary freely between $[-1, 1]$
 165 which allows the argument α to be unconstrained in terms of its values in radians. The interpolating
 166 function $w(\cdot)$ is defined as $w(z) = \max(0, |z| - 1)$.

167 These binning functions conform a trilinear interpolation that has a combined effect of sharing the
 168 contribution of each oriented gradient between their eight adjacent bins in a tridimensional cube in the
 169 histogram space, and zero everywhere else.

170 Lastly, the fixed value of 3 is a magnification factor which corresponds to the number of pixels per each
 171 block when $s = 1$. As the patch has 16 blocks and 8 bin angles are considered, for each location l and
 172 channel c a feature called *descriptor* $\mathbf{d}^{(l,c)}$ of 128 dimension is obtained.

173 Figure 3 shows an example of a patch and a scheme of the histogram computation. In (A) a plot of the
 174 signal and the patch centered around the keypoint is shown. In (B) the possible orientations on each patch
 175 are illustrated. Only the upper-left four blocks are visible. The first eight orientations of the first block, are
 176 labeled from 1 to 8 clockwise. The orientations of the second block $B_{1,2}$ are labeled from 9 to 16. This
 177 labeling continues left-to-right, up-down until the eight orientations for all the sixteen blocks are assigned.
 178 They form the corresponding descriptor \mathbf{d} of 128 coordinates. Finally, in (C) an enlarged image plot is
 179 shown where the oriented gradient vector for each pixel can be seen.

180 2.1.4 Speller Matrix letter Identification

181 2.1.4.1 P300 ERP Extraction

182 Segments corresponding to row flickering are labeled 1-6, whereas those corresponding to column
 183 flickering are labeled 7-12. The extraction process has the following steps:

- 184 • **Step A:** First highlight rows and columns from the matrix in a random permutation order and obtain
 185 the Ensemble Average as detailed in steps 1, 2 and 3 in Section 2.1.1.
- 186 • **Step B:** Plot the signals $\tilde{x}^l(n, c)$, $1 \leq n \leq n_{\text{max}}$, $1 \leq c \leq C$, according Section 2.1.2 in order to
 187 generate the images $I^{(l,c)}$ for rows and columns $1 \leq l \leq 12$.
- 188 • **Step C:** Obtain the descriptors $\mathbf{d}^{(l,c)}$ for rows and columns from $I^{(l,c)}$ in accordance to the method
 189 described in Section 2.1.3.

190 2.1.4.2 Calibration

191 A trial, as defined by the BCI2000 platform (Schalk et al., 2004), is every attempt to select just one letter
 192 from the speller. A set of trials is used for calibration and once the calibration is complete it can be used to
 193 identify new letters from new trials.

194 During the calibration phase, two descriptors $\mathbf{d}^{(l,c)}$ are extracted for each available channel, corresponding
 195 to the locations l of a selection of one previously instructed letter from the set of calibration trials. These
 196 descriptors are the P300 templates, grouped together in a template set called T^c . The set is constructed
 197 using the steps described in Section 2.1.1 and the steps A, B and C of the P300 ERP extraction process.

198 Additionally, the best performing channel, bpc is identified based on the the channel where the best
 199 Character Recognition Rate is obtained.

200 **2.1.4.3 Letter identification**

201 In order to identify the selected letter, the template set T^{bpc} is used as a database. Thus, new descriptors
 202 are computed and they are compared against the descriptors belonging to the calibration template set T^{bpc} .

203 • **Step D:** Match to the calibration template T^{bpc} by computing

$$\hat{row} = \arg \min_{l \in \{1, \dots, 6\}} \sum_{q \in N_T(\mathbf{d}^{(l,bpc)})} \left\| q - \mathbf{d}^{(l,bpc)} \right\|^2 \quad (8)$$

204 and

$$\hat{col} = \arg \min_{l \in \{7, \dots, 12\}} \sum_{q \in N_T(\mathbf{d}^{(l,bpc)})} \left\| q - \mathbf{d}^{(l,bpc)} \right\|^2 \quad (9)$$

205 where $N_T(\mathbf{d}^{(l,bpc)})$ is defined as $N_T(\mathbf{d}^{(l,bpc)}) = \{\mathbf{d} \in T^{bpc} / \mathbf{d}$ is the k-nearest neighbor of $\mathbf{d}^{(l,bpc)}$ } for
 206 the best performing channel. This set is obtained by sorting all the elements in T^{bpc} based on distances
 207 between them and $\mathbf{d}^{(l,bpc)}$, choosing the k with smaller values, with k a parameter of the algorithm.
 208 This procedure is based on the k-NBNN algorithm (Boiman et al., 2008).

209 By computing the aforementioned equations, the letter of the matrix can be determined from the intersection
 210 of the row \hat{row} and column \hat{col} . Figure 2 shows a scheme of this process.

211 **2.2 Experimental Protocol**

212 To verify the validity of the proposed framework and method, the public dataset 008-2014 (Riccio et al.,
 213 2013) published on the BNCI-Horizon website (Brunner et al., 2014) by IRCCS Fondazione Santa Lucia,
 214 is used. Additionally, an own dataset with the same experimental conditions is generated. Both of them are
 215 utilized to perform an offline BCI Simulation to decode the spelled words from the provided signals.

216 The algorithm is implemented using VLFeat (Vedaldi and Fulkerson, 2010) Computer Vision libraries
 217 on MATLAB V2014a (Mathworks Inc., Natick, MA, USA). Furthermore, in order to enhance the impact
 218 of our paper and for a sake of reproducibility, the code of the algorithm has been made available at:
 219 <https://bitbucket.org/itba/hist>.

220 In the following sections the characteristics of the datasets and parameters of the identification algorithm
 221 are described.

222 **2.2.1 P300 ALS Public Dataset**

223 The experimental protocol used to generate this dataset is explained in (Riccio et al., 2013) but can
 224 be summarized as follows: 8 subjects with confirmed diagnoses but on different stages of ALS disease,
 225 were recruited and accepted to perform the experiments. The Visual P300 detection task designed for this
 226 experiment consisted of spelling 7 words of 5 letters each, using the traditional P300 Speller Matrix (Farwell
 227 and Donchin, 1988). The flashing of rows and columns provide the deviant stimulus required to elicit this
 228 physiological response. The first 3 words are used for calibration and the remaining 4 words, for testing
 229 with visual feedback. A trial is every attempt to select a letter from the speller. It is composed of signal
 230 segments corresponding to $k_a = 10$ repetitions of flashes of 6 rows and $k_a = 10$ repetitions of flashes of

231 6 columns of the matrix, yielding 120 repetitions. Flashing of a row or a column is performed for 0.125
 232 s, following by a resting period (i.e. inter-stimulus interval) of the same length. After 120 repetitions an
 233 inter-trial pause is included before resuming with the following letter.

234 The recorded dataset was sampled at 256 Hz and it consisted of a scalp multichannel EEG signal for
 235 electrode channels Fz, Cz, Pz, Oz, P3, P4, PO7 and PO8, identified according to the 10-20 International
 236 System, for each one of the 8 subjects. The recording device was a research-oriented digital EEG device
 237 (g.Mobilab, g.Tec, Austria) and the data acquisition and stimuli delivery were handled by the BCI2000
 238 open source software (Schalk et al., 2004).

239 In order to assess and verify the identification of the P300 response, subjects are instructed to perform a
 240 copy-spelling task. They have to fix their attention to successive letters for copying a previously determined
 241 set of words, in contrast to a free-running operation of the speller where each user decides on its own what
 242 letter to choose.

243 2.2.2 P300 for healthy subjects

244 We replicate the same experiment on healthy subjects using a wireless digital EEG device (g.Nautilus,
 245 g.Tec, Austria). The experimental conditions are the same as those used for the previous dataset, as detailed
 246 in section 2.2.1. The produced dataset is available in a public online repository (Ramele et al., 2017).

247 Participants are recruited voluntarily and the experiment is conducted anonymously in accordance with
 248 the Declaration of Helsinki published by the World Health Organization. No monetary compensation
 249 is handed out and all participants agree and sign a written informed consent. This study is approved
 250 by the *Departamento de Investigación y Doctorado, Instituto Tecnológico de Buenos Aires (ITBA)*. All
 251 healthy subjects have normal or corrected-to-normal vision and no history of neurological disorders. The
 252 experiment is performed with 8 subjects, 6 males, 2 females, 6 right-handed, 2 left-handed, average age
 253 29.00 years, standard deviation 11.56 years, range 20-56 years.

254 EEG data is collected in a single recording session. Participants are seated in a comfortable chair, with
 255 their vision aligned to a computer screen located one meter in front of them. The handling and processing
 256 of the data and stimuli is conducted by the OpenVibe platform (Renard et al., 2010).

257 Gel-based active electrodes (g.LADYbird, g.Tec, Austria) are used on the same positions Fz, Cz, Pz,
 258 Oz, P3,P4, PO7 and PO8. Reference is set to the right ear lobe and ground is preset as the AFz position.
 259 Sampling frequency is slightly different, and is set to 250 Hz, which is the closest possible to the one used
 260 with the other dataset.

261 2.2.3 Parameters

262 The patch size is $X_P = 12s \times 12s$ pixels, where s is the scale of the local patch and it is an input parameter
 263 of the algorithm. The P300 event can have a span of 400 ms and its amplitude can reach $10\mu V$ (Rao, 2013).
 264 Hence it is necessary to utilize a signal segment of size $t_{max} = 1$ second and a size patch X_P that could
 265 capture an entire transient event. With this purpose in consideration, the s value election is essential.

266 We propose the Equations 10 and 11 to compute the scale value in horizontal and vertical directions,
 267 respectively.

$$s_x = \frac{\gamma \lambda F_s}{12} \quad (10)$$

$$s_y = \frac{\gamma \Delta \mu V}{12} \quad (11)$$

where λ is the length in seconds covered by the patch, F_s is the sampling frequency of the EEG signal (downsampled to 16 Hz) and $\Delta\mu V$ corresponds to the amplitude in microvolts that can be covered by the height of the patch. The geometric structure of the patch forces a squared configuration, then we discerned that by using $s = s_x = s_y = 3$ and $\gamma = 4$, the local patch and the descriptor can identify events of $9 \mu V$ of amplitude, with a span of $\lambda = 0.56$ seconds. This also determines that 1 pixel represents $\frac{1}{\gamma} = \frac{1}{4}\mu V$ on the vertical direction and $\frac{1}{F_s \gamma} = \frac{1}{64}$ seconds on the horizontal direction. The keypoints p_k are located at $(x_{p_k}, y_{p_k}) = (0.55F_s \gamma, z^l(c)) = (35, z^l(c))$ for the corresponding channel c and location l (see Equation 4). In this way the whole transient event is captured. Figure 4 shows a patch of a signal plot covering the complete amplitude (vertical direction) and the complete span of the signal event (horizontal direction).

Lastly, the number of channels C is equal to 8 for both datasets, and the number of intensification sequences k_a is fixed to 10. The parameter k used to construct the set $N_T(\mathbf{d}^{(l,c)})$ is assigned to $k = 7$, which was found empirically to achieve better results. In addition, the norm used on Equations 8 and 9 is the cosine norm, and descriptors are normalized to $[-1, 1]$.

3 RESULTS

Table 1 shows the results of applying the Histogram of Gradient Orientations (HIST) algorithm to the subjects of the public dataset of ALS patients. The percentage of correctly spelled letters is calculated while performing an offline BCI Simulation. From the seven words for each subject, the first three are used for calibration, and the remaining four are used for testing. The best performing channel bpc is informed as well. The target ratio is 1 : 36; hence theoretical chance level is 2.8%. It can be observed that the best performance of the letter identification method is reached in a dissimilar channel depending on the subject being studied. This table shows for comparison the obtained performance rates using single-channel signals with the Support Vector Machine (SVM) (Scholkopf and Smola, 2001) classifier. This method is configured to use a linear kernel. The best performing channel, where the best letter identification rate was achieved, is also depicted.

The Information Transfer Rate (ITR), or Bit Transfer Rate (BTR), in the case of reactive BCIs (Wolpaw and E., 2012) depends on the amount of signal averaging required to transmit a valid and robust selection. Figure 5 shows the performance curves for varying intensification sequences for the subjects included in the dataset of ALS patients. It can be noticed that the percentage of correctly identified letters depends on the number of intensification sequences that are used to obtain the averaged signal. Moreover, when the number of intensification sequences tend to 1, which corresponds to single-intensification character recognition, the performance is reduced. As mentioned before, the SNR of the P300 obtained from only one segment of the intensification sequence is very low and the shape of its P300 component is not very well defined.

In Table 2 the results obtained for 8 healthy subjects are shown. It can be observed that the performance is above chance level. It was verified that HIST method has an improved performance at letter identification than SVM that process the signals on a channel by channel strategy (Wilcoxon signed-rank test, $p = 0.004$ for both datasets).

Tables 3 and 4 are presented in order to compare the performance of the HIST method versus a multichannel version of the Stepwise Linear Discriminant Analysis (SWLDA) and SVM classification algorithms for both datasets. The feature was formed by concatenating all the channels (Krusienski et al., 2006). SWLDA is the methodology proposed by the ALS dataset's publisher. Since authors Riccio et al. (2013) did not report the Character Recognition Rate obtained for this dataset, we replicate their procedure

309 and include the performance obtained with the SWLDA algorithm at letter identification. It was verified for
310 the dataset of ALS patients that it has similar performance against other methods like SWLDA or SVM,
311 which use a multichannel feature (Quade test with $p = 0.55$) whereas for the dataset of healthy subjects
312 significant differences were found (Quade test with $p = 0.02$) where only the HIST method achieved a
313 different performance than SVM (with multiple comparisons, significant difference of level 0.05).

314 The P300 ERP consists of two overlapping components: the P3a and P3b, the former with frontocentral
315 distribution while the latter stronger on centroparietal region (Polich, 2007). Hence, the standard practice is
316 to find the stronger response on the central channel Cz (Riccio et al., 2013). However, Krusienski et al.
317 (2006) show that the response may also arise in occipital regions. We found that by analyzing only the
318 waveforms, occipital channels PO8 and PO7 show higher performances for some subjects.

319 As subjects have varying *latencies* and *amplitudes* of their P300 components, they also have a varying
320 stability of the *shape* of the generated ERP (Nam et al., 2010). Figure 6 shows 10 sample P300 templates
321 patches for patients 8 and 3 from the dataset of ALS patients. It can be discerned that in coincidence with
322 the performance results, the P300 signature is more clear and consistent for subject 8 (A) while for subject
323 3 (B) the characteristic pattern is more difficult to perceive.

324 Additionally, the stability of the P300 component waveform has been extensively studied in patients
325 with ALS (Sellers et al., 2006; Madarame et al., 2008; Nijboer and Broermann, 2009; Mak et al., 2012;
326 McCane et al., 2015) where it was found that these patients have a stable P300 component, which were
327 also sustained across different sessions. In line with these results we do not find evidence of a difference in
328 terms of the performance obtained by analyzing the waveforms (HIST) for the group of patients with ALS
329 and the healthy group of volunteers (Mann-Whitney U Test, $p = 0.46$). Particularly, the best performance
330 is obtained for a subject from the ALS dataset for which, based on visual observation, the shape of their
331 P300 component is consistently identified.

332 It is important to remark that when applied to binary images obtained from signal plots, the feature
333 extraction method described in Section 2.1.3 generates sparse descriptors. Under this subspace we found
334 that using the cosine metric yielded a significant performance improvement. On the other hand, the unary
335 classification scheme based on the NBNN algorithm proved very beneficial for the P300 Speller Matrix.
336 This is due to the fact that this approach solves the unbalance dataset problem which is inherent to the
337 oddball paradigm (Tibon and Levy, 2015).

4 DISCUSSION

338 Among other applications of Brain Computer Interfaces, the goal of the discipline is to provide
339 communication assistance to people affected by neuro-degenerative diseases, who are the most likely
340 population to benefit from BCI systems and EEG processing and analysis.

341 In this work, a method to extract an objective metric from the waveform of the plots of EEG signals is
342 presented. Its usage to implement a valid P300-Based BCI Speller application is expounded. Additionally,
343 its validity is evaluated using a public dataset of ALS patients and an own dataset of healthy subjects.

344 It was verified that this method has an improved performance at letter identification than other methods
345 that process the signals on a channel by channel strategy, and it even has a comparable performance against
346 other methods like SWLDA or SVM, which uses a multichannel feature. Furthermore, this method has the
347 advantage that shapes of waveforms can be analyzed in an objective way. We observed that the shape of
348 the P300 component is more stable in occipital channels, where the performance for identifying letters

349 is higher. We additionally verified that ALS P300 signatures are stable in comparison to those of healthy
350 subjects.

351 We believe that the use of descriptors based on histogram of gradient orientation, presented in this work,
352 can also be utilized for deriving a shape metric in the space of the P300 signals which can complement
353 other metrics based on time-domain as those defined by Mak et al. (2012). It is important to notice
354 that the analysis of waveform shapes is usually performed in a qualitative approach based on visual
355 inspection (Sellers et al., 2006), and a complementary methodology which offer a quantitative metric will
356 be beneficial to these routinely analysis of the waveform of ERPs.

357 The goal of this work is to answer the question if a P300 component could be solely determined by
358 inspecting automatically their waveforms. We conclude affirmatively, though two very important issues
359 still remain:

360 First, the stability of the P300 in terms of its shape is crucial: the averaging procedure, montages, the
361 signal to noise ratio and spatial filters all of them are non-physiological factors that affect the stability of
362 the shape of the P300 ERP. We tested a preliminary approach to assess if the morphological shape of the
363 P300 of the averaged signal can be stabilized by applying different alignments of the stacked segments (see
364 Figure 2) and we verified that there is a better performance when a correct segment alignment is applied.
365 We applied Dynamic Time Warping (DTW) (Casarotto et al., 2005) to automate the alignment procedure
366 but we were unable to find a substantial improvement. Further work to study the stability of the shape of
367 the P300 signature component needs to be addressed.

368 The second problem is the amplitude variation of the P300. We propose a solution by standardizing the
369 signal, shown in Equation 2. It has the effect of normalizing the peak-to-peak amplitude, moderating its
370 variation. It has also the advantage of reducing noise that was not reduced by the averaging procedure. It is
371 important to remark that the averaged signal variance depends on the number of segments used to compute
372 it (Van Drongelen, 2006). The standardizing process converts the signal to unit signal variance which
373 makes it independent of the number k_a of signals averaged. Although this is initially an advantageous
374 approach, the standardizing process reduces the amplitude of any significant P300 complex diminishing its
375 automatic interpretation capability.

376 In our opinion, the best benefit of the presented method is that a closer collaboration of the field of BCI
377 with physicians can be fostered (Chavarriaga et al., 2017), since this procedure intent to imitate human
378 visual observation. Automatic classification of patterns in EEG that are specifically identified by their
379 shapes like K-Complex, Vertex Waves, Positive Occipital Sharp Transient (Hartman, 2005) are a prospect
380 future work to be considered. We are currently working in unpublished material analyzing K-Complex
381 components that could eventually provide assistance to physicians to locate these EEG patterns, specially in
382 long recording periods, frequent in sleep research (Michel and Murray, 2012). Additionally, it can be used
383 for artifact removal which is performed on many occasions by visually inspecting signals. This is due to
384 the fact that the descriptors are a direct representation of the shape of signal waveforms. In line with these
385 applications, it can be used to build a database (Chavarriaga et al., 2017) of quantitative representations of
386 waveforms and improve atlases (Hartman, 2005), which are currently based on qualitative descriptions of
387 signal shapes.

CONFLICT OF INTEREST STATEMENT

388 The authors declare that the research was conducted in the absence of any commercial or financial
389 relationships that could be construed as a potential conflict of interest.

AUTHOR CONTRIBUTIONS

390 This work is part of the PhD thesis of RR which is directed by JS and codirected by AV.

FUNDING

391 This project was supported by the ITBACyT-15 funding program issued by ITBA University from Buenos
392 Aires, Argentina.

REFERENCES

- 393 Alvarado-González, M., Garduño, E., Bribiesca, E., Yáñez-Suárez, O., and Medina-Bañuelos, V. (2016).
394 P300 Detection Based on EEG Shape Features. *Computational and Mathematical Methods in Medicine*,
395 1–14doi:10.1155/2016/2029791
- 396 Berger, S., Schneider, G., Kochs, E., and Jordan, D. (2017). Permutation Entropy: Too Complex a Measure
397 for EEG Time Series? *Entropy* 2017, Vol. 19, Page 692 19, 692. doi:10.3390/E19120692
- 398 Boiman, O., Shechtman, E., and Irani, M. (2008). In defense of nearest-neighbor based image classification.
399 *26th IEEE Conference on Computer Vision and Pattern Recognition, CVPR* doi:10.1109/CVPR.2008.
400 4587598
- 401 Bresenham, J. E. (1965). Algorithm for computer control of a digital plotter. *IBM Systems Journal* 4,
402 25–30
- 403 Brunner, C., Blankertz, B., Cincotti, F., Kübler, A., Mattia, D., Miralles, F., et al. (2014). BNCI Horizon
404 2020 – Towards a Roadmap for Brain / Neural Computer Interaction. *Lecture Notes in Computer Science*
405 8513, 475–486
- 406 Carlson, T. and del R. Millan, J. (2013). Brain-controlled wheelchairs: A robotic architecture. *IEEE
407 Robotics & Automation Magazine* 20, 65–73. doi:10.1109/MRA.2012.2229936
- 408 Casarotto, S., Bianchi, A., Cerutti, S., and Chiarenza, G. (2005). Dynamic time warping in the analysis of
409 event-related potentials. *IEEE Engineering in Medicine and Biology Magazine* 24, 68–77. doi:10.1109/
410 MEMB.2005.1384103
- 411 Chavarriaga, R., Fried-Oken, M., Kleih, S., Lotte, F., and Scherer, R. (2017). Heading for new shores!
412 Overcoming pitfalls in BCI design. *Brain-Computer Interfaces* 4, 60–73. doi:10.1080/2326263X.2016.
413 1263916
- 414 Clerc, M., Bougrain, L., and Lotte, F. (2016). *Brain-computer interfaces, Technology and applications
415 2(Cognitive Science)* (ISTE Ltd. and Wiley)
- 416 De Vos, M. and Debener, S. (2014). Mobile EEG: Towards brain activity monitoring during natural action
417 and cognition. *International Journal of Psychophysiology* 91, 1–2. doi:10.1016/j.ijpsycho.2013.10.008
- 418 Edelman, S., Intrator, N., and Poggio, T. (1997). Complex cells and object recognition
- 419 Farwell, L. A. and Donchin, E. (1988). Talking off the top of your head: toward a mental prosthesis utilizing
420 event-related brain potentials. *Electroencephalography and clinical neurophysiology* 70, 510–23
- 421 Guger, C., Allison, B. Z., and Lebedev, M. A. (2017). Introduction. In *Brain Computer Interface Research:
422 A State of the Art Summary* 6 (Springer, Cham). 1–8. doi:10.1007/978-3-319-64373-1_1
- 423 Guger, C., Daban, S., Sellers, E., Holzner, C., Krausz, G., Carabalona, R., et al. (2009). How many people
424 are able to control a P300-based brain-computer interface (BCI)? *Neuroscience Letters* 462, 94–98.
425 doi:10.1016/j.neulet.2009.06.045
- 426 Hartman, a. L. (2005). *Atlas of EEG Patterns*, vol. 65 (Lippincott Williams & Wilkins). doi:10.1212/01.
427 wnl.0000174180.41994.39

- 428 Hu, L., Mouraux, A., Hu, Y., and Iannetti, G. D. (2010). A novel approach for enhancing the signal-to-noise
429 ratio and detecting automatically event-related potentials (ERPs) in single trials. *NeuroImage* 50, 99–111.
430 doi:10.1016/j.neuroimage.2009.12.010
- 431 Huggins, J. E., Alcaide-Aguirre, R. E., and Hill, K. (2016). Effects of text generation on P300 brain-
432 computer interface performance. *Brain-Computer Interfaces* 3, 112–120. doi:10.1080/2326263X.2016.
433 1203629
- 434 Jure, F., Carrere, L., Gentiletti, G., and Tabernig, C. (2016). BCI-FES system for neuro-rehabilitation of
435 stroke patients. *Journal of Physics: Conference Series* 705, 1–8. doi:10.1088/1742-6596/705/1/012058
- 436 Knuth, K. H., Shah, A. S., Truccolo, W. A., Ding, M., Bressler, S. L., and Schroeder, C. E. (2006).
437 Differentially variable component analysis: Identifying multiple evoked components using trial-to-trial
438 variability. *Journal of Neurophysiology* 95, 3257–3276. doi:10.1152/jn.00663.2005
- 439 Krusienski, D. J., Sellers, E. W., Cabestaing, F., Bayoudh, S., McFarland, D. J., Vaughan, T. M., et al.
440 (2006). A comparison of classification techniques for the P300 Speller. *Journal of Neural Engineering*
441 3, 299–305. doi:10.1088/1741-2560/3/4/007
- 442 Liang, N. and Bougrain, L. (2008). Averaging techniques for single-trial analysis of oddball event-related
443 potentials. *4th International Brain-Computer*, 1–6
- 444 Lotte, F., Faller, J., Guger, C., Renard, Y., Pfurtscheller, G., Lécuyer, A., et al. (2013). *Combining BCI*
445 *with Virtual Reality: Towards New Applications and Improved BCI* (Berlin, Heidelberg: Springer Berlin
446 Heidelberg). 197–220. doi:10.1007/978-3-642-29746-5_10
- 447 Lowe, G. (2004). SIFT - The Scale Invariant Feature Transform. *International Journal* 2, 91–110
- 448 Madarame, T., Tanaka, H., Inoue, T., Kamata, M., and Shino, M. (2008). The development of a brain
449 computer interface device for amyotrophic lateral sclerosis patients. In *Conference Proceedings - IEEE*
450 *International Conference on Systems, Man and Cybernetics* (IEEE), 2401–2406. doi:10.1109/ICSMC.
451 2008.4811654
- 452 Mak, J. N., McFarland, D. J., Vaughan, T. M., McCane, L. M., Tsui, P. Z., Zeitlin, D. J., et al. (2012). EEG
453 correlates of P300-based brain-computer interface (BCI) performance in people with amyotrophic lateral
454 sclerosis. *Journal of Neural Engineering* 9. doi:10.1088/1741-2560/9/2/026014
- 455 McCane, L. M., Heckman, S. M., McFarland, D. J., Townsend, G., Mak, J. N., Sellers, E. W., et al.
456 (2015). P300-based brain-computer interface (BCI) event-related potentials (ERPs): People with
457 amyotrophic lateral sclerosis (ALS) vs. age-matched controls. *Clinical Neurophysiology* 126, 2124–2131.
458 doi:10.1016/j.clinph.2015.01.013
- 459 Michel, C. M. and Murray, M. M. (2012). Towards the utilization of EEG as a brain imaging tool.
460 *NeuroImage* 61, 371–385. doi:10.1016/j.neuroimage.2011.12.039
- 461 Nam, C. S., Li, Y., and Johnson, S. (2010). Evaluation of P300-based brain-computer interface in real-
462 world contexts. *International Journal of Human-Computer Interaction* 26, 621–637. doi:10.1080/
463 10447311003781326
- 464 Nijboer, F. and Broermann, U. (2009). Brain Computer Interfaces for Communication and Control in
465 Locked-in Patients. In *Graimann B., Pfurtscheller G., Allison B. (eds) Brain-Computer Interfaces. The*
466 *Frontiers Collection*. (Springer Berlin Heidelberg). 185–201. doi:10.1007/978-3-642-02091-9_11
- 467 Novak, D., Sigrist, R., Gerig, N. J., Wyss, D., Bauer, R., Gotz, U., et al. (2018). Benchmarking brain-
468 computer interfaces outside the laboratory: The cybathlon 2016. *Frontiers in Neuroscience* 11, 756.
469 doi:10.3389/fnins.2017.00756
- 470 Polich, J. (2007). Updating P300: An integrative theory of P3a and P3b. *Clinical Neurophysiology* 118,
471 2128–2148. doi:10.1016/j.clinph.2007.04.019

- 472 Ramele, R., Villar, A. J., and Santos, J. M. (2016). BCI classification based on signal plots and SIFT
473 descriptors. In *4th International Winter Conference on Brain-Computer Interface, BCI 2016* (Yongpyong:
474 IEEE), 1–4. doi:10.1109/IWW-BCI.2016.7457454
- 475 [Dataset] Ramele, R., Villar, A. J., and Santos, J. M. (2017). P300-dataset rrid scr_015977.
476 <https://www.kaggle.com/ramele/p300samplingdataset>
- 477 Rao, R. P. N. (2013). *Brain-Computer Interfacing: An Introduction* (New York, NY, USA: Cambridge
478 University Press)
- 479 Renard, Y., Lotte, F., Gibert, G., Congedo, M., Maby, E., Delannoy, V., et al. (2010). OpenViBE: An
480 Open-Source Software Platform to Design, Test, and Use Brain-Computer Interfaces in Real and Virtual
481 Environments. *Presence: Teleoperators and Virtual Environments* 19, 35–53. doi:10.1162/pres.19.1.35
- 482 Riccio, A., Simione, L., Schettini, F., Pizzimenti, A., Inghilleri, M., Belardinelli, M. O., et al. (2013).
483 Attention and P300-based BCI performance in people with amyotrophic lateral sclerosis. *Frontiers in
484 Human Neuroscience* 7, 732. doi:10.3389/fnhum.2013.00732
- 485 Riener, R. and Seward, L. J. (2014). Cybathlon 2016. *2014 IEEE International Conference on Systems,
486 Man, and Cybernetics (SMC)*, 2792–2794doi:10.1109/SMC.2014.6974351
- 487 Schalk, G., McFarland, D. J., Hinterberger, T., Birbaumer, N., and Wolpaw, J. R. (2004). BCI2000: a
488 general-purpose brain-computer interface (BCI) system. *IEEE transactions on bio-medical engineering*
489 51, 1034–43. doi:10.1109/TBME.2004.827072
- 490 Scholkopf, B. and Smola, A. J. (2001). *Learning with kernels: support vector machines, regularization,
491 optimization, and beyond* (MIT press)
- 492 Schomer, D. L. and Silva, F. L. D. (2010). *Niedermeyer's Electroencephalography: Basic Principles,
493 Clinical Applications, and Related Fields* (Walters Klutter -Lippincott Williams & Wilkins)
- 494 Sellers, E. W., Kübler, A., and Donchin, E. (2006). Brain-computer interface research at the University of
495 South Florida cognitive psychophysiology laboratory: The P300 speller. *IEEE Transactions on Neural
496 Systems and Rehabilitation Engineering* 14, 221–224. doi:10.1109/TNSRE.2006.875580
- 497 Tibon, R. and Levy, D. A. (2015). Striking a balance: analyzing unbalanced event-related potential data.
498 *Frontiers in psychology* 6, 555. doi:10.3389/fpsyg.2015.00555
- 499 Van Drongelen, W. (2006). *Signal processing for neuroscientists: an introduction to the analysis of
500 physiological signals* (Academic press)
- 501 Vedaldi, A. and Fulkerson, B. (2010). VLFeat - An open and portable library of computer vision algorithms.
502 *Design* 3, 1–4. doi:10.1145/1873951.1874249
- 503 Wolpaw, J. and E., W. (2012). *Brain-Computer Interfaces: Principles and Practice* (Oxford University
504 Press)
- 505 Yamaguchi, T., Fujio, M., Inoue, K., and Pfurtscheller, G. (2009). Design method of morphological
506 structural function for pattern recognition of EEG signals during motor imagery and cognition. In *Fourth
507 International Conference on Innovative Computing, Information and Control (ICICIC)*. 1558–1561.
508 doi:10.1109/ICICIC.2009.161

Table 1. Character recognition rates for the public dataset of ALS patients using the Histogram of Gradient (HIST) calculated from single-channel plots. Performance rates using single-channel signals with the SVM classifier are shown for comparison. The best performing channel *bpc* for each method is visualized

Participant	<i>bpc</i>	HIST	<i>bpc</i>	Single Channel SVM
1	Cz	35%	Cz	15%
2	Fz	85%	PO8	25%
3	Cz	25%	Fz	5%
4	PO8	55%	Oz	5%
5	PO7	40%	P3	25%
6	PO7	60%	PO8	20%
7	PO8	80%	Fz	30%
8	PO7	95%	PO7	85%

Table 2. Character recognition rates for the own dataset of healthy subjects using the Histogram of Gradient (HIST) calculated from single-channel plots. Performance rates using single-channel signals with the SVM classifier are shown for comparison. The best performing channel *bpc* for each method is visualized.

Participant	<i>bpc</i>	HIST	<i>bpc</i>	Single Channel SVM
1	Oz	40%	Cz	10%
2	PO7	30%	Cz	5%
3	P4	40%	P3	10%
4	P4	45%	P4	35%
5	P4	60%	P3	10%
6	Pz	50%	P4	25%
7	PO7	70%	P3	30%
8	P4	50%	PO7	10%

Table 3. Character recognition rates and the best performing channel *bpc* for the public dataset of ALS patients using the Histogram of Gradient (HIST) (repeated here for comparison purposes). Performance rates obtained by SWLDA and SVM classification algorithms with a multichannel concatenated feature.

Participant	<i>bpc</i> for HIST	HIST	Multichannel SWLDA	Multichannel SVM
1	Cz	35%	45%	40%
2	Fz	85%	30%	50%
3	Cz	25%	65%	55%
4	PO8	55%	40%	50%
5	PO7	40%	35%	45%
6	PO7	60%	35%	70%
7	PO8	80%	60%	35%
8	PO7	95%	90%	95%

Table 4. Character recognition rates and the best performing channel *bpc* for the own dataset of healthy subjects using the Histogram of Gradient (HIST) (repeated here for comparison purposes). Performance rates obtained by SWLDA and SVM classification algorithms with a multichannel concatenated feature.

Participant	<i>bpc</i> for HIST	HIST	Multichannel SWLDA	Multichannel SVM
1	Oz	40%	65%	40%
2	PO7	30%	15%	10%
3	P4	40%	50%	25%
4	P4	45%	40%	20%
5	P4	60%	30%	20%
6	Pz	50%	35%	30%
7	PO7	70%	25%	30%
8	P4	50%	35%	20%

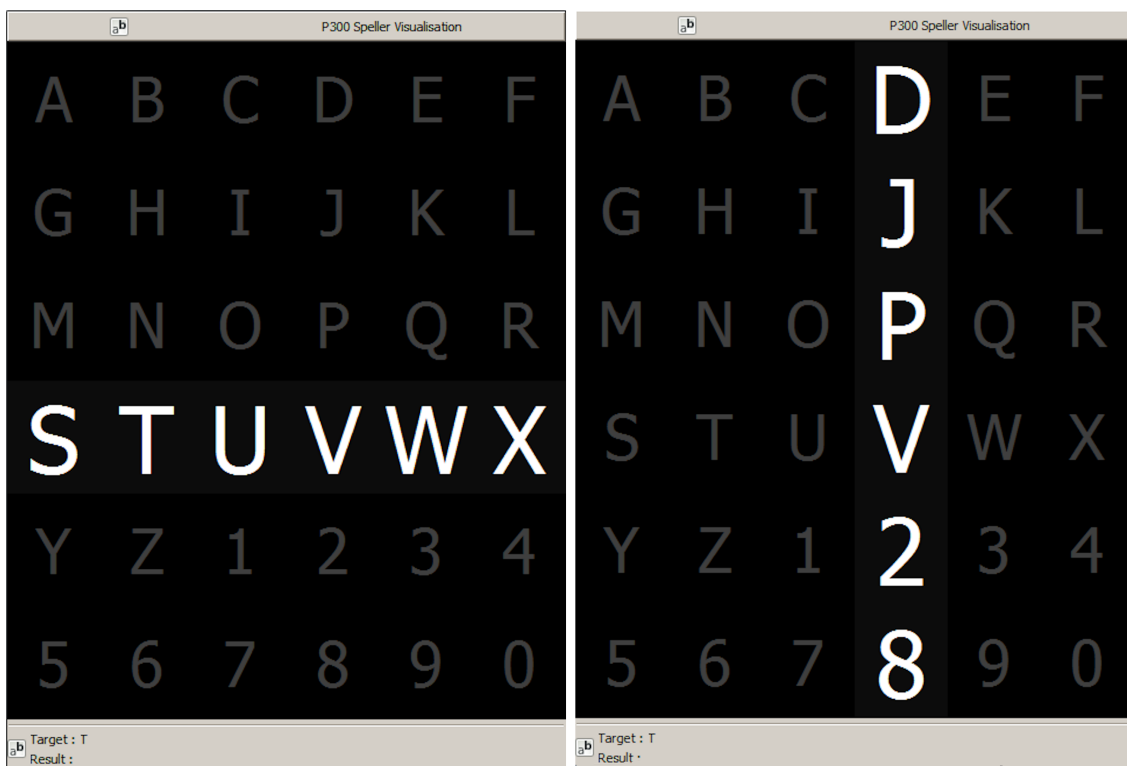


Figure 1. Example of the 6×6 Speller Matrix used in the study obtained from the OpenVibe software. Rows and columns flash in random permutations.

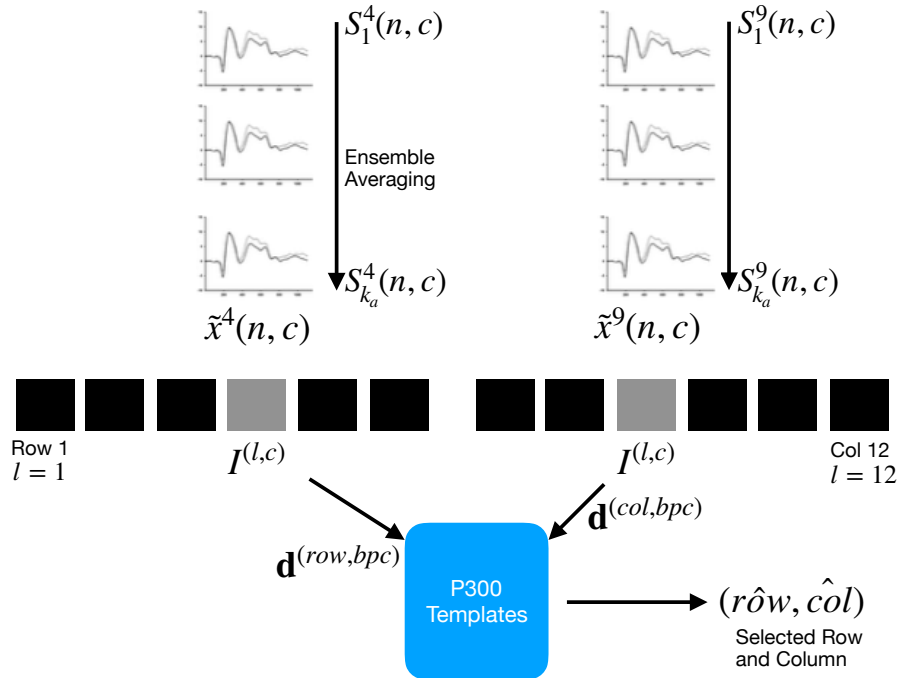


Figure 2. For each column and row, an averaged, standardized and scaled signal $\tilde{x}^l(n, c)$ is obtained from the segments S_i^l corresponding to the k_a intensification sequences with $1 \leq i \leq k_a$ and location l varying between 1 and 12. From the averaged signal, the image $I^{(l,c)}$ of the signal plot is generated and each descriptor is computed. By comparing each descriptor against the set of templates, the P300 ERP can be detected, and finally the desired letter from the matrix can be inferred.

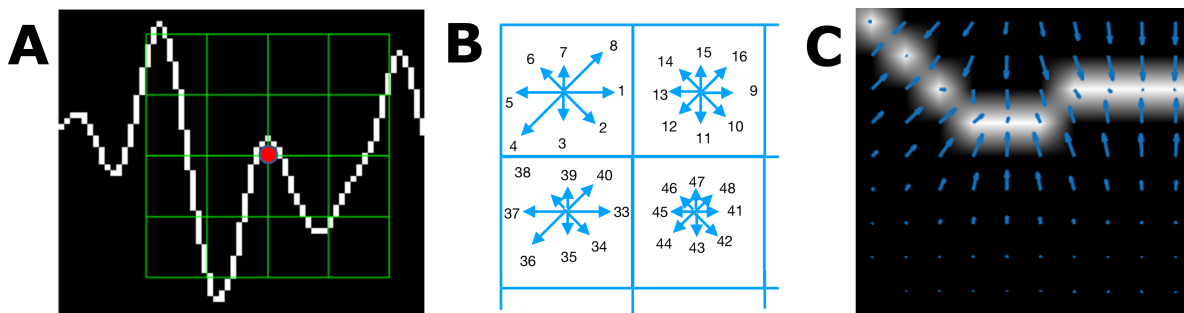


Figure 3. (A) Example of a plot of the signal, a keypoint and the corresponding patch. (B) A scheme of the orientation's histogram computation. Only the upper-left four blocks are visible. The first eight orientations of the first block, are labeled from 1 to 8 clockwise. The orientation of the second block $B_{1,2}$ is labeled from 9 to 16. This labeling continues left-to-right, up-down until the eight orientations for all the sixteen blocks are assigned. They form the corresponding descriptor of 128 coordinates. The length of each arrow represent the value of the histogram on each direction for each block. (C) Vector field of oriented gradients. Each pixel is assigned an orientation and magnitude calculated using finite differences.

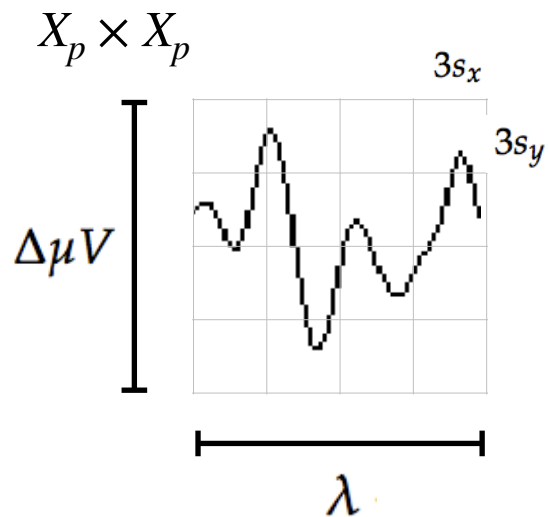


Figure 4. The scale of local patch is selected in order to capture the whole transient event. The size of the patch is $X_p \times X_p$ pixels. The vertical size consists of 4 blocks of size $3s_y$ pixels which is high enough as to contain the signal $\Delta\mu V$, the peak-to-peak amplitude of the transient event. The horizontal size includes 4 blocks of $3s_x$ and covers the entire duration in seconds of the transient signal event, λ .

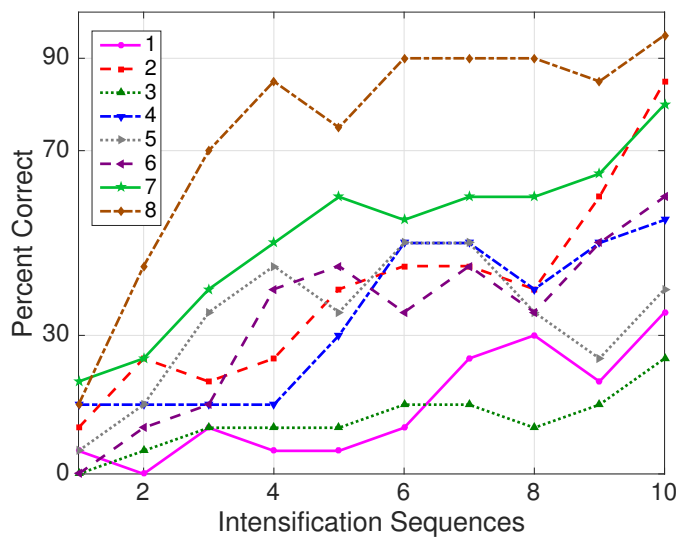


Figure 5. Performance curves for the eight subjects included in the dataset of ALS patients. Three out of eight subjects achieved the necessary performance to implement a valid P300 speller.

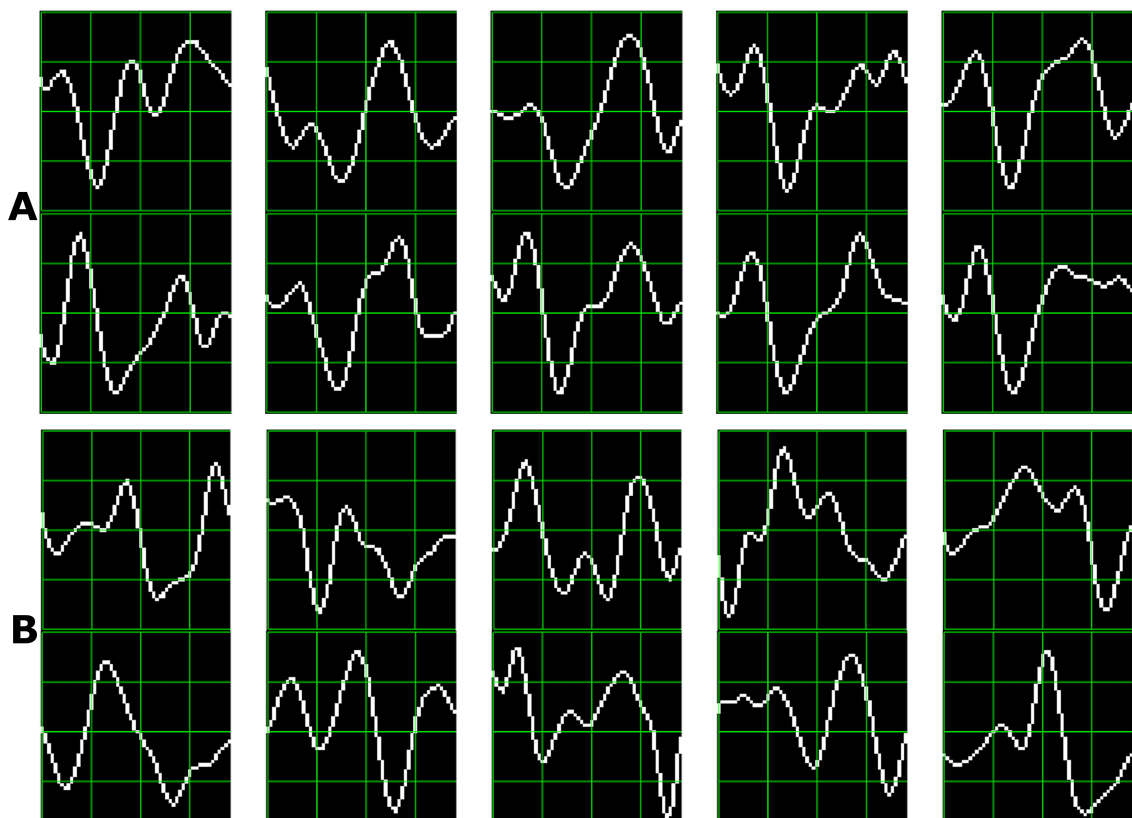


Figure 6. Ten sample P300 template patches for subjects 8 (A) and 3 (B) of the ALS Dataset. Downward deflection is positive polarity.